J Ginseng Res 44 (2020) 461–474

Contents lists available at ScienceDirect

Journal of Ginseng Research

journal homepage: http://www.ginsengres.org

Research Article

Protein target identification of ginsenosides in skeletal muscle tissues: discovery of natural small-molecule activators of muscle-type creatine kinase

Feiyan Chen [1,5,☆], Kexuan Zhu [1,2,☆], Lin Chen [3,☆], Liufeng Ouyang [1,4], Cuihua Chen [5], Ling Gu [5], Yucui Jiang [5], Zhongli Wang [6], Zixuan Lin [1], Qiang Zhang [1], Xiao Shao [1], Jianguo Dai [1], Yunan Zhao [1,5,*]

[1] Department of Pathology and Pathophysiology, School of Medicine and Life Science, Nanjing University of Chinese Medicine, Nanjing, China
[2] Hanlin College, Nanjing University of Chinese Medicine, Taizhou, China
[3] Department of Physiology, School of Medicine and Life Science, Nanjing University of Chinese Medicine, Nanjing, China
[4] Laboratory of Pathological Sciences, College of Medicine, Yan'an University, Yan'an, China
[5] Research Center, Basic Medical College, Nanjing University of Chinese Medicine, Nanjing, China
[6] School of Nursing, Jiujiang University, Jiujiang, China

ARTICLE INFO

Article history:
Received 31 December 2018
Received in Revised form
19 February 2019
Accepted 27 February 2019
Available online 7 March 2019

Keywords:
Affinity chromatography
Creatine kinase
Fatigue
Ginseng
20(S)-protopanaxadiol

ABSTRACT

Background: Ginseng effectively reduces fatigue in both animal models and clinical trials. However, the mechanism of action is not completely understood, and its molecular targets remain largely unknown.
Methods: By screening for proteins that interact with the primary components of ginseng (ginsenosides) in an affinity chromatography assay, we have identified muscle-type creatine kinase (CK-MM) as a potential target in skeletal muscle tissues.
Results: Biolayer interferometry analysis showed that ginsenoside metabolites, instead of parent ginsenosides, had direct interaction with recombinant human CK-MM. Subsequently, 20(S)-protopanaxadiol (PPD), which is a ginsenoside metabolite and displayed the strongest interaction with CK-MM in the study, was selected as a representative to confirm direct binding and its biological importance. Biolayer interferometry kinetics analysis and isothermal titration calorimetry assay demonstrated that PPD specifically bound to human CK-MM. Moreover, the mutation of key amino acids predicted by molecular docking decreased the affinity between PPD and CK-MM. The direct binding activated CK-MM activity *in vitro* and *in vivo*, which increased the levels of tissue phosphocreatine and strengthened the function of the creatine kinase/phosphocreatine system in skeletal muscle, thus buffering cellular ATP, delaying exercise-induced lactate accumulation, and improving exercise performance in mice.
Conclusion: Our results suggest a cellular target and an initiating molecular event by which ginseng reduces fatigue. All these findings indicate PPD as a small molecular activator of CK-MM, which can help in further developing better CK-MM activators based on the dammarane-type triterpenoid structure.

1. Introduction

Ginseng, the root of *Panax ginseng* Meyer, is one of the most popular and valuable medicinal plants throughout the world [1]. In traditional Chinese medicine, ginseng was used as a tonic that was believed to replenish energy. Today, ginseng is distributed to different countries in various forms and consumed as a dietary supplement to improve general well-being, physical stamina, and concentration [2]. It occupies a prominent position on the list of the best-selling medicinal plants in the world [3]. In addition, the world ginseng market is estimated to be worth $2 billion in 2013 [4]. The recognized primary active components of ginseng are a series of tetracyclic triterpenoid saponins, also referred to as ginsenosides. To date, more than 40 ginsenosides have been identified and

* Corresponding author. Department of Pathology and Pathophysiology, School of Medicine and Life Science, Nanjing University of Chinese Medicine, Nanjing, 210046, China.
E-mail address: zhaoyunan-js@163.com (Y. Zhao).
☆ These authors contributed equally to this work.

https://doi.org/10.1016/j.jgr.2019.02.005
p1226-8453 e2093-4947/$ – see front matter

isolated from ginseng, which can be mainly classified into two groups on the basis of the chemical structure of their aglycones: the protopanaxatriol group (e.g., Rg1, Re, Rh1, and Rf) and the protopanaxadiol group (e.g., Rb1, Rb2, Rc, Rd, Rg3, and Rh2) (Supplementary Fig. 1) [2,5]. In general, the ginsenosides Rg1, Re, Rb1, Rb2, Rc, and Rd are the six major saponins in ginseng. Ginsenosides are metabolized extensively by intestinal bacteria after oral administration. In the protopanaxadiol group, Rb1 and Rd are biotransformed into 20(S)-protopanaxadiol (PPD) via Rh2 and ginsenoside compound K (GK). In the protopanaxatriol group, Rg1 and Re are converted into 20(S)-protopanaxatriol (PPT) via Rh1 and F1 [6,7]. After oral ingestion, parent ginsenosides and their metabolites, which are thought to contribute to the herb's claimed health-related properties, are absorbed from the gut into the systemic circulation.

The tonic effects of ginseng are believed to reduce fatigue and enhance physical performance. Ma et al [8] reported that ginseng extract supplementation improved exercise performance and decreased fatigue-associated parameters in mice. Ginseng extract supplementation can dose-dependently increase endurance swimming time in a weight-loaded swimming test and decrease the levels of serum lactate after the acute exercise challenge. Oh et al [9] showed that ginseng water extract exhibits antifatigue activity in mice as reflected by the physiological markers for physical fatigue and that the antifatigue effect of ginseng is attributable to its saponins rather than to its polysaccharides. In addition, ginseng extract or ginsenosides can alleviate psychological and postoperative fatigue in rodent animals [10,11]. In clinical trials, Lee et al [12] and Kim et al [13] provided the first evidence of the antifatigue effects of ginseng extract in healthy adults and patients with idiopathic chronic fatigue by using a randomized, double-blind, placebo-controlled, and parallel-designed trial. To date, two systematic reviews of clinical trials showed modest support for ginseng as treatment for fatigue [14,15]. According to a meta-analysis performed by Bach et al [16], there was statistically significant efficacy of ginseng on fatigue reduction, but a definitive conclusion could not be formed because only few randomized controlled trials with a small sample size have been published so far.

Some possible biological mechanisms are responsible for the efficacy of ginseng on fatigue relief, including increased hemoglobin levels, enhanced oxygen extraction by muscles, and improved mitochondrial metabolism in the muscle [17,18]. However, the mechanisms have not been fully understood, and specifically, the exact action targets of ginseng still remain unclear. Thus, the aim of the present study is to identify the direct protein targets of ginsenosides and the initiating events triggered by primary components of ginseng to provide high-quality evidence for the use of ginseng on reducing fatigue.

In this study, we immobilized ginseng total saponins onto 4% cross-linked agarose beads with covalent-linked diaminodipropylamine and performed affinity chromatography, which is a classical method for target identification [19] and to screen for protein targets of ginsenosides in skeletal muscle tissues. Here, we identified nearly 40 potential protein targets including muscle-type creatine kinase (CK-MM). We used biolayer interferometry (BLI) to assess the direct interaction between ginsenosides and CK-MM and found that their metabolites instead of parent ginsenosides displayed direct interaction with CK-MM. The interaction of PPD, as a representative, with CK-MM was further validated through BLI kinetics analysis, isothermal titration calorimetry (ITC) assay, and molecular docking assay. Importantly, PPD can activate CK-MM activity *in vitro* and *in vivo*. This process enhanced the function of the CK/phosphocreatine (PCr) system in skeletal muscle, improved cellular energy metabolism, and retarded exercise-induced lactate accumulation, reducing fatigue and improving exercise performance in mice.

2. Methods

2.1. Preparation of high-purity ginseng total saponins

High-purity ginseng total saponins were prepared as described in our previous report [20]. The ginsenosides Rg1, Re, Rh1, Rg2, Rc, Rb2, Rb3, Rd, F2, and Rg3 were detected in high-purity ginseng total saponins (Supplementary Fig. 2). The estimated contents of total saponins were approximately 107% and 90% according to the colorimetric method and charged aerosol detection response, respectively [21]. Rg1, Re, Rh1, Rb1, F1, Rd, Rh2, GK, PPT, and PPD standards (purity $>$ 98%) were purchased from the National Institutes for Food and Drug Control (Beijing, China).

2.2. Affinity chromatography

First, the protocol to synthesize ginsenoside–bead conjugate was modified from the study by Joo et al. [22]. In brief, 80% ethanol solution (0.35 mL) of high-purity ginseng total saponins (5 mg) was added dropwise into a solution (0.25 mL) containing $NaIO_4$ (2 mg). An equal volume of 40% ethanol solution of sucrose (3 mg) was used as the negative control. The solution was stirred at room temperature for 1 h. Then, 0.5 mL of carbonate buffer (100 mM, pH = 9.0) was added to the solution. The mixture was transferred to centrifuge columns (5 mL; Thermo Pierce, Boston , USA) containing 0.5 mL of Carboxylink Coupling Gel (Thermo Pierce), and the columns were inverted several times before incubating at room temperature for 1 h. Subsequently, 0.375 mL of $NaBH_4$ solution (4 mg/mL) was added to the mixture, which was then incubated and shaken at room temperature for 4 h. Then, the columns were centrifuged at 1000 rpm for 30 s to remove the medium, and the beads were further washed three times with deionized water.

Second, 400 mg of fresh mouse muscle tissues was homogenized with 4 mL of ice-cold RIPA (Radio Immunoprecipitation Assay Sigma, Burlington, USA) lysis buffer containing 1 mM phenylmethylsulfonyl fluoride (Sigma). The homogenate was centrifuged at 12,000 rpm for 10 min at 4 °C. The supernatant (1.5 mL) was incubated overnight with the resulting ginsenoside-linked beads at 4 °C, followed by extensive washing with RIPA buffer to remove nonspecifically bound proteins. The tightly binding proteins on beads were then denatured in 350 μL sample buffer (1% sodium dodecyl sulfate [SDS], 1% dithiothreitol [Sigma], 10 mM Tris-HCl, 10% glycerol, 1 mM EDTA, pH ≈ 8.0) at 95 °C for 5 min. After centrifuging at 1000 rpm for 30 s, the eluate was collected and stored at −20 °C.

Third, 15 μL of each sample was separated by SDS polyacrylamide gel electrophoresis (SDS-PAGE) on 10% polyacrylamide gels. After one-dimensional gel separation, the gels were stained with 0.1% Coomassie Blue R250 (Sigma) in 10% acetic acid, 50% methanol, and 40% H_2O for 1 h. The gels were subsequently destained by soaking for at least 2 h in 10% acetic acid, 50% methanol, and 40% H_2O with at least two changes of this solvent until the background was nearly clear. Finally, the target bands were cut out and identified by liquid chromatography coupled to tandem mass spectrometry. Protein identification was carried out through the technical services provided by Fitgene Biotech (Guangzhou, China) (http://www.fitgene.com/), which included in-gel digestion, peptide enrichment, peptide cleanup, mass spectrometry [23], and Mascot analysis [24] (Matrix Science, London, UK, http://www.matrixscience.com/search_intro.html).

2.3. Biolayer interferometry

An Octet RED96 system (ForteBio, Menlo Park, CA, USA) was used to measure the binding of small molecules to wild-type (WT) or mutant forms of human CK-MM [25]. The detailed procedures

are described in the Supplementary Methods. The association (K_{on}) and dissociation (Ko_{ff}) curves were fitted using a single exponential fitting model. The final K_{on} and Ko_{ff} rate constants were used to calculate the affinity ($K_D = Ko_{ff}/K_{on}$). All experiments were carried out in triplicate.

2.4. Isothermal titration calorimetry

The thermodynamic parameters for the binding of PPD and recombinant human CK-MM (Sigma) were determined by ITC (Macrocal iTC200; Malvern, USA) [26]. The cell and syringe were filled with 50 μM CK-MM in phosphate buffer saline (PBS) buffer containing 5% dimethyl sulfoxide (DMSO) and 500 μM PPD in PBS buffer containing 5% DMSO, respectively. Each experiment consisted of a single 2 μL injection of PPD solution into the CK-MM solution at room temperature. An equal volume of vehicle was used as the negative control of injection. Data analysis was performed with the software package Origin 5.0, OriginLab, Northampton, USA. The integrated heats generated in the experiments were fitted assuming a single-site binding model.

2.5. Molecular docking

Molecular docking was performed using Schrödinger software, New York, USA (http://www.schrodinger.com) and FTMap server, Boston, USA (http://ftmap.bu.edu/login.php). We downloaded the three-dimensional structure of PPD (PubChem CID: 11213350) from the National center for biotechnology information (NCBI) PubChem Compound database (http://www.ncbi.nlm.nih.gov/pccompound) and the monomeric crystal structure of human CK-MM (PDB ID: 1I0E) from the research collaboratory for structure bioinformatics (RCSB) Protein Data Bank (http://www.rcsb.org/pdb). By using the SiteMap tool of Schrödinger software and FTMap server, the potential binding sites on the surface of CK-MM were predicted. The Glide tool of Schrödinger software was then used to perform docking simulation of CK-MM and PPD with the default setting. The docking conformation of PPD at each potential binding site was scored by the GlideScore tool. The best binding conformation at the active site was analyzed by covering the known key amino acid residues involved in H-bonds, hydrophobic interactions, and van der Waals forces.

2.6. Site-directed mutagenesis based on overlap extension polymerase chain reaction

A CK-MM open reading frame (ORF) was amplified using the primers (Supplementary Table 1) and cDNA of human cardiomyocyte cells (HCM) cells (Bena Culture Collection, Beijing, China) as a template. The amplicon was digested with BamHII and XhoI and cloned into BamHI/XhoI-digested expression vector pET-28a to generate pET10. Using site-directed mutagenesis with pET10 as template, pET11, pET12, and pET13 were constructed, which have mutations of glutamine at Position 318 to proline (CK-MM Q318P, Mutant 1) (Supplementary Fig. 3), arginine at Position 320 to threonine (CK-MM R320T, Mutant 2) (Supplementary Fig. 4), and serine at Position 285 to threonine (CK-MM S285T, Mutant 3) (Supplementary Fig. 5), respectively.

2.7. Protein expression and purification

Escherichia coli BL-21 cells were transformed with the plasmid (pET10, pET11, pET12, or pET13) to express recombinant His-tagged CK-MM. The detailed procedures are described in the Supplementary Methods. The protein purity was evaluated by SDS-PAGE on 10% polyacrylamide gels under denaturing conditions using protein marker (Bio-Rad, California, USA) as a reference protein for molecular mass estimation (Supplementary Fig. 6).

2.8. Experimental animals

Male institute of cancer research (ICR) mice weighing 18–22 g each were purchased from SLAC Laboratory Animal Co., Ltd. (Shanghai, China). These mice were housed on a standard 12-h light/dark cycle (lights on between 7:00 and 19:00 h) with ad libitum access to food and water at a constant temperature of 25 °C ± 1 °C. The animals were housed in groups of five per cage and allowed to habituate for 1 week. All animal procedures were approved by the Institutional Animal Care and Use Committee of Nanjing University of Chinese Medicine and carried out in accordance with the Guidelines of Accommodation and Care for Animals formulated by the Chinese Convention for the Protection of Vertebrate Animals Used for Experimental and Other Scientific Purposes. The minimum number of animals required to obtain consistent data was used.

2.9. Procedures

Animal Experiment 1: effects of PPD on CK-MM activity and PCr content in skeletal muscle

The mice were randomly assigned to four experimental groups (n = 10/group): control group, 25 mg/kg/day PPD group, 50 mg/kg/day PPD group, and 100 mg/kg/day PPD group. PPD (Jingke Chemical Science and Technology Corporation, Shanghai, China) was suspended in physiological saline containing 1% carboxymethyl cellulose and administered daily by gastric gavages, whereas the control group of mice was given the vehicle only. Three dosages of PPD were based on previous pharmacokinetic reports that it could produce a plasma peak concentration of 3–10 μM in rodent animals after profess to be convinced (p.o.) administration once with 100 mg/kg PPD [53]. After treatment for 3 weeks, the mice were anesthetized using sodium pentobarbital and flash-frozen through rapid immersion in liquid nitrogen. Afterward, the skeletal muscle tissues from the hind limbs were collected and immediately pulverized under liquid nitrogen using a mortar and pestle for enzyme activity assay, CK-MM protein and mRNA expression analysis, and PCr assay.

Animal Experiment 2: effects of PPD on exercise performance in a weight-loaded swimming test

The mice were randomly assigned to four experimental groups (n = 10/group): control group, 25 mg/kg/day PPD group, 50 mg/kg/day PPD group, and 100 mg/kg/day PPD group. After daily p.o. administration for 3 weeks, the mice were subjected to the weight-loaded swimming test. Briefly, after each mouse was weighed, a lead block (10% of the body weight) was loaded onto its tail. Then, the mice were dropped individually in 35 cm of ambient temperature water (25 ± e °C) in a plastic pool (40 × 25 × 25 cm). The swimming endurance time of each mouse was recorded from the beginning up to exhaustion, which was determined as a loss of coordinated movements and failure to return to the surface within 7 s.

Animal Experiment 3: preventive effects of PPD on energy metabolism during intense exercise

The animals were randomly divided into four experimental groups: control group (n = 10), control + PPD group (n = 10), swim group (n = 10), and swim + PPD group (n = 10). The experiment consisted of two phases. The first experimental phase lasted for 3 weeks. During this phase, the mice of the control + PPD and swim + PPD groups received PPD (100 mg/kg/day, suspended in physiological saline containing 1% carboxymethyl cellulose) orally. The animals of the control and swim groups were administrated orally with the vehicle. The second experimental phase consisted of

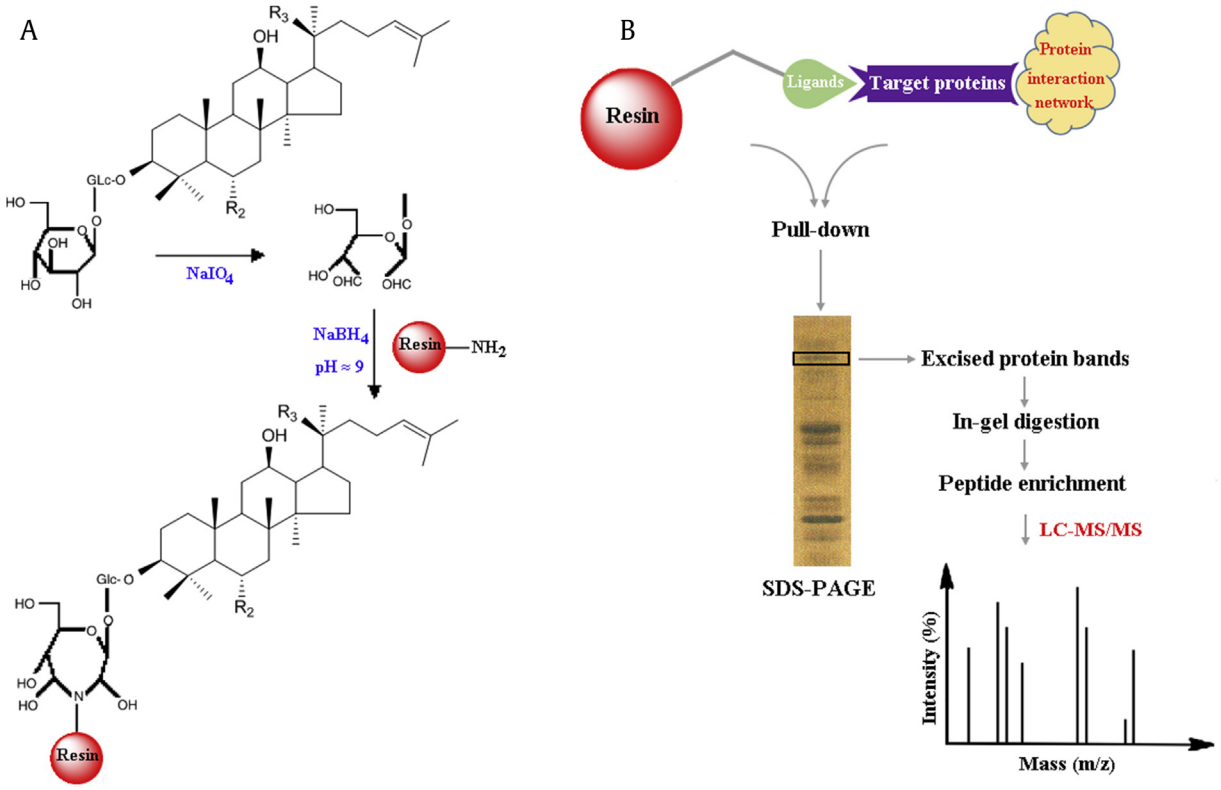

Fig. 1. General workflow of small-molecule affinity chromatography. (A) Ginsenosides are immobilized to the resin by the sodium periodate oxidation method. (B) Protein lysates are incubated with the matrix–ligand chemical complex to enrich target proteins. Unbound proteins are washed away, followed by elution of the target proteins under highly denaturing conditions. Eluted mixtures containing the target proteins can be assessed by SDS-PAGE and LC–MS/MS analysis. LC–MS/MS; liquid chromatography coupled to tandem mass spectrometry; SDS-PAGE, sodium dodecyl sulfate polyacrylamide gel electrophoresis.

intense exercise for 90 s. The mice of the swim and swim + PPD groups were submitted to the weight-loaded swimming as described previously. Afterward, the mice were anesthetized using diethyl ether and flash-frozen through rapid immersion in liquid nitrogen. The skeletal muscle tissues from the hind limbs were then collected and immediately pulverized under liquid nitrogen for lactate assay and PCr and adenine nucleotide analysis by high-performance liquid chromatography (HPLC).

2.10. Lactate assay

The powdered skeletal muscle tissues (400 mg) were homogenized with 1 mL of 0.5 M perchloric acid. The homogenate was centrifuged at 12,000 rpm for 10 min at 4 °C. Lactate and total protein concentration in the supernatant were measured using the commercial kits (Catalog Nos. A019-2 and A045-3; Jiancheng Bioengineering Institute, China) as per the manufacturer's protocol. The unknown sample concentration was determined from the standard curve and expressed as mmol lactate per mg protein. The mean value of the triplicate readings for each sample was calculated.

2.11. Enzyme activity assay

The powdered skeletal muscle tissues were weighed (100 mg) and homogenized with 1 mL of ice-cold RIPA lysis buffer. The homogenate was centrifuged at 12,000 rpm for 10 min at 4 °C. Up to 20 μL of the supernatant was used for CK-MM activity analysis following the manufacturer's protocol (Catalog No. A032; Jiancheng Bioengineering Institute, China). CK-MM activity in unknown samples was calculated using the standard curve of purified mouse CK-MM (Life Diagnostics, West Chester, USA) and was expressed as U/g skeletal muscle tissue. For *in vitro* CK-MM activation assay, 20 μL of the supernatant was replaced with 10 μL of different final concentrations of compound (0–80 μM) and 10 μL of purified mouse (Life Diagnostics), recombinant human (Sigma), or purified rabbit (Sigma) CK-MM. All measurements were carried out in triplicate.

2.12. Western blot and real-time polymerase chain reaction analysis

The protocol for western blot and real-time polymerase chain reaction was identical to the one described previously [27]. The primary antibodies included rabbit polyclonal anti–CK-MM (1:2000; Sangon Biotech, Shanghai, China) and rabbit polyclonal anti–β-tubulin (1:500; Proteintech, PA, USA). The secondary antibody used was horseradish peroxidase–conjugated goat anti–rabbit IgG (1:10,000; GeneScript, Nanjing, China).The polymerase chain reaction primers of mouse RPS18 endogenous reference genes were purchased from Sangon Biotech (Shanghai, China). The sequences of primers for CK-MM were as follows: forward: 5′-AGACAAGCATAAGACCGACCTCAACCACG-3′, reverse: 5′-ACCTCCTTCATATTGCCTCCCTTCTCCAT-3′. Ten animals per group were included in this analysis, and the data were obtained with triplicates.

2.13. Determination of PCr, ADP, and ATP in the skeletal muscle tissues

The protocol to determine PCr, ADP, and ATP was modified from the studies by Xu et al [28] and Di Pierro et al [29]. Briefly, the powdered skeletal muscle tissues were weighed (400 mg) and homogenized with 1 mL of 0.5 M perchloric acid. The homogenate was centrifuged at 10,000 rpm for 20 min at 4 °C. The resultant

A

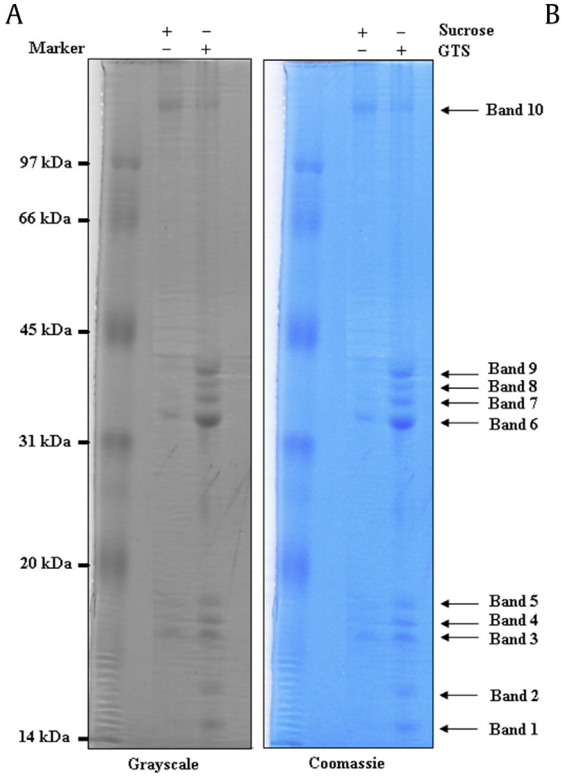

B

Bands	Potential proteins		
	Description	Sequence coverage	Score
Band 9	actin (gi|4501881, Mass: 42366)	34%	200
Band 8	actin (gi|4501881, Mass: 42366)	59%	78
Band 7	creatine kinase M-type (gi|6671762, Mass: 43246)	38%	173
Band 5	troponin I (gi|7949078, Mass: 20954)	41%	76
Band 4	myosin regulatory light chain 2 (gi|7949078, Mass: 19057)	72%	191
Band 2	myosin light chain 1/3 (gi|164664497, Mass: 16703)	33%	77
Band 1	unnamed protein product (gi|12846961, Mass: 14443)	69%	112

Fig. 2. Protein target identification of ginsenosides in skeletal muscle tissues using affinity chromatography. (A) Ginseng total saponins (GTSs) were adopted as the ligand, whereas the negative control pull-down adopted sucrose as the ligand. Eluted mixtures were visualized by one-dimensional SDS-PAGE with Coomassie staining. The bands whose abundance differed between the GTS and control samples were cut out and identified by peptide fragment analysis using LC–MS/MS. (B) Mass spectrometric data were converted into Mascot generic format and then analyzed by Mascot search engine (Matrix Science) to identify proteins from peptide sequence databases. The most potential protein for each band was listed based on the Mascot score and sequence coverage. LC–MS/MS; liquid chromatography coupled to tandem mass spectrometry; SDS-PAGE, sodium dodecyl sulfate polyacrylamide gel electrophoresis.

supernatant was neutralized with 5 M NaOH solution. Up to 25 μL of the supernatant was used for the HPLC coupled to ultraviolet spectrometry analysis. The chromatographic separation conditions, HPLC system, and representative chromatograms are described in Supplementary Fig. 7 and Supplementary Fig. 8. The concentrations of PCr, ATP, and ADP in the supernatant were calculated from the standard curves. The PCr, ATP, and ADP levels in the skeletal muscle tissues were expressed as nmol/g skeletal muscle tissue.

2.14. Statistical analysis

Data were expressed as mean ± standard error of mean for the indicated number of experiments and analyzed using the Statistical Package for Social Sciences computer program version 10.1, IBM, New York, USA. For Animal Experiments 1 and 2, differences among groups were analyzed by one-way analysis of variance (ANOVA). For Animal Experiment 3, statistical significance was determined by two-way ANOVA with treatment and swim as independent, between-subject factors. In case of significant interactions, Tukey's honest significant difference test of multiple comparisons was performed. The two-tailed Pearson test was used for correlation analysis. The significance level was set at $P \leq 0.05$ for all statistical comparisons.

3. Results

3.1. Target primary screening of ginsenosides in skeletal muscle tissues by affinity chromatography

High-purity ginseng total saponins including Rg1, Re, Rf, F3, Rh1, Rg2, Rb1, Rc, Rb2, Rb3, Rd, Rg3, and F2 were adopted as the ligand, and their glycosyl sites were used as points of attachment to the resin by the sodium periodate oxidation method (Fig. 1A). Then, the compound-linked beads were incubated with skeletal muscle tissue extracts, followed by extensive washing to remove nonspecifically bound proteins. The tightly binding proteins were eluted under highly denaturing conditions and were subsequently analyzed by SDS-PAGE (Fig. 1B). Ten protein bands were shown on one-dimensional SDS-PAGE stained with Coomassie Blue, whereas the negative control pull-down, which adopted sucrose as the ligand, displayed three protein bands (Bands 3, 6, and 10) on one-dimensional SDS-PAGE (Fig. 2A). Seven other protein bands (Bands 1, 2, 4, 5, 7, 8, and 9) were cut out, digested with trypsin, and identified by liquid chromatography coupled to tandem mass spectrometry. Seventy proteins were identified by Mascot search engine and are shown in Supplementary Figs. 9–15. After filtering out the repeated hits, we finally identified nearly 40 proteins as potential targets of ginsenosides. Potential target proteins with top Mascot score for each band were unknown protein product (Supplementary Fig. 16), myosin light chain 1/3 (Supplementary Fig. 17), myosin light chain 2 (Supplementary Fig. 18), troponin I (Supplementary Fig. 19), CK-MM (Supplementary Fig. 20), and actin (Supplementary Figs. 21 and 22) (Fig. 2B). Given that brain-type CK was also identified as a potential target of ginsenosides in brain tissues (Supplementary Fig. 23), the direct interaction between CK-MM and ginsenosides was confirmed as a matter of priority in subsequent studies. As for five other potential target proteins with top Mascot score, we have not confirmed the direct binding to ginsenosides.

3.2. PPD bound directly to recombinant human CK-MM

The direct binding was first determined using BLI, wherein human CK-MM was immobilized on a biosensor, and a wavelength

shift was measured in real time after addition or dilution of a small molecule. At the concentration of 300 μM, the direct binding response of CK-MM to Rg1, Re, Rb1, Rd, Rh1, F1, Rh2, GK, PPT, and PPD is shown in Fig. 3A and Supplementary Fig. 24. Ginsenosides including Rg1, Re, Rb1, Rd, and Rh1 almost have no direct interaction with CK-MM. With the decrease of the polarity and sugar molecules, F1, Rh2, K, and their aglycones (PPT and PPD) displayed gradually direct interaction with CK-MM. Among them, PPD (Fig. 3B) had the strongest direct binding to CK-MM and was selected as a representative for the following affinity and binding conformation analysis.

The BLI technique can determine the rates of intermolecular K_{on}, Ko_{ff}, and binding constants (e.g., $K_D = Ko_{ff}/K_{on}$) [30]. BLI kinetics analysis revealed that PPD had the affinity (K_D) for human CK-MM of 2.53 ± 0.12E-5 M. The K_{on} and Ko_{ff} rates of PPD for CK-MM were 4.24 ± 0.21E3 1/Ms and 1.07 ± 0.10E-1 1/s, respectively (Fig. 3C). To further confirm the direct binding of PPD to CK-MM and evaluate the physicochemical parameters of this interaction, we performed an ITC assay, which can measure the affinity of binding partners in their native states [31]. PPD (500 μM) was titrated into 50 μM CK-MM solution. The K_D value of the interaction was 1.9 ± 0.30E-6 M, determined by two independent experiments and calculated with a well-fitting to 1:1 binding model. The thermodynamic parameters for the interaction indicated that it was enthalpy driven with a small preferable entropy component (ΔH = −3494 ± 95.07 cal/mol and ΔS = 14.5 cal/mol/deg) (Fig. 3D).

3.3. Molecular docking analysis of CK-MM and PPD

Then, we performed a molecular docking analysis to investigate the binding site of CK-MM/PPD complex based on the published monomeric crystal structure of human CK-MM (PDB ID: 1I0E). CK-MM is a member of the kinase family [32], and the ADP binding pocket (S1″) is its natural site (Fig. 4A). Considering the distinct structural difference between PPD and ADP/kinase inhibitors, we first explored other potential active sites in the crystal structure of CK-MM by FTMap (Fig. 4A) and SiteMap (Fig. 4B) software analysis. Besides the ADP binding site (S1″), we explored another potential active site (S2″) adjacent to the S1″ site. GlideScore analysis showed that the absolute value of docking conformation score at the S2″ site was greater than that at the S1″ site (Fig. 4C). Consequently, PPD was likely to bind to the S2″ site and was docked successively into the active site by Glide software analysis. The search algorithm was used to sequentially adjust the orientation, position, and

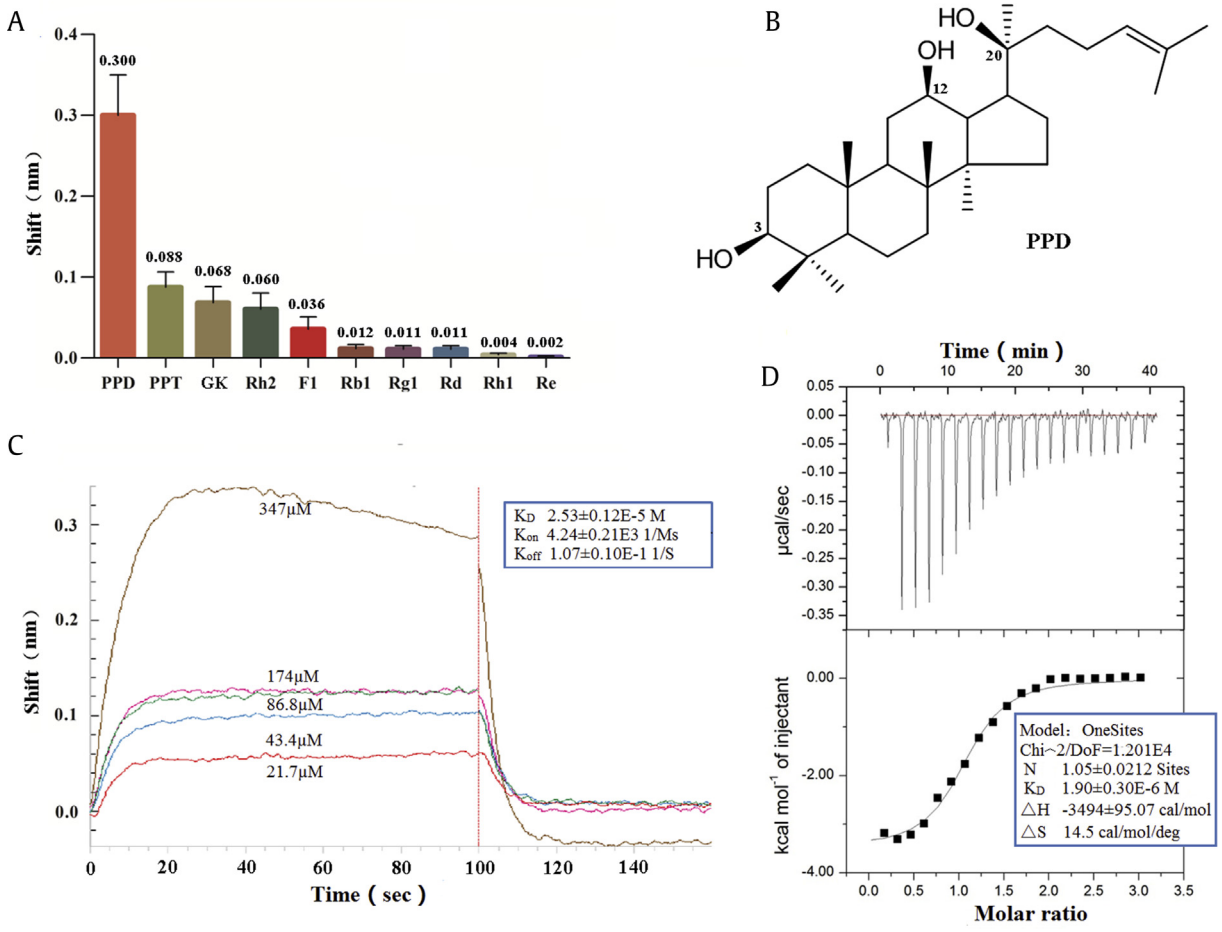

Fig. 3. Direct interaction between recombinant human CK-MM and ginsenosides. (A) Direct binding response of CK-MM to ginsenosides and their aglycones (PPT and PPD) was determined using the BLI technique (mean ± SEM, $n = 3$). (B) Chemical structure of PPD is shown, which had the strongest direct binding to CK-MM. (C) BLI kinetics analysis of the binding of PPD to CK-MM. Streptavidin-coated biosensors were loaded with biotinylated CK-MM and then incubated with PPD to generate an association curve. The 60-s association phase was subsequently followed by a 90-s dissociation step. The results presented are representative of at least three experiments. (D) ITC measurements for CK-MM binding to PPD. The upper panel shows the representative titration thermograms, and the lower panel shows the data integration with fitted curves (1:1 binding model) of PPD with CK-MM. ITC data shown are representative of two replicates and reported ± the error of fitting. BLI, biolayer interferometry; CK-MM, muscle-type creatine kinase; GK, ginsenoside compound K; ITC, isothermal titration calorimetry; PPT, protopanaxatriol; PPD, 20(S)-protopanaxadiol; SEM, standard error of mean.

conformation of PPD to find the best conformation that could better bind CK-MM. The results showed that PPD with two electronegative groups (3-OH and 12-OH) generated three hydrogen bond (H-bond) interactions with the S2″ site amino acid residues and appeared well adapted to the S2″ pocket (Fig. 4D). 3-OH formed two H-bonds with Arg320 (R320) and Gln318 (Q318), whereas 12-OH formed one H-bond with Ser285 (S285) (Supplementary Fig. 25).

3.4. Q318 residue was critical for CK-MM/PPD complex

Based on the predicted key amino acids (Q318, R320, and S285) in the S2″ site, we generated a mutant human CK-MM (CK-MM Q318P, Mutant 1) using site-directed mutagenesis, where glutamine at Position 318 was mutated to proline. Similarly, another mutant (CK-MM R320T, Mutant 2) was generated, in which arginine at Position 320 was mutated to threonine. With regard to the third mutant (CK-MM S285T, Mutant 3), we mutated serine at Position 285 to threonine (Fig. 5A). BLI was used to detect the affinity of WT and mutant forms of CK-MM to PPD. The results showed that the K_D values of WT, Mutant 1, Mutant 2, and Mutant 3 were 2.37 ± 0.11E-5 M (Fig. 5B), 3.09 ± 0.11E-2 M (Fig. 5C), 5.14 ± 0.13E-4 M (Fig. 5D), and 9.56 ± 0.10E-5 M (Fig. 5E), respectively. The affinity of WT to PPD was approximately 1300, 20, and 4 times higher than that of Mutant 1, Mutant 2, and Mutant 3 to PPD, respectively (Fig. 5F). These data indicated that PPD directly bound to the S2″ site of CK-MM. In addition, Mutant 1 displayed a weak interaction with PPD, suggesting that the Q318 residue was critical for the binding of CK-MM to PPD.

3.5. CK-MM activity in vitro

Three ginsenosides (Rg1, Rd, and Rh2) and two aglycones (PPT and PPD) were selected as representatives to observe their effects on CK-MM activity. The results are shown in Fig. 6. In general, PPD, PPT, and Rh2 significantly increased CK-MM activity and showed an inverted U-shaped effect. In addition, significant correlations were observed between the maximum increase rate of enzyme activity and the small molecule−enzyme interaction ($r = 0.989$, $P = 0.001$, $n = 5$) (Supplementary Fig. 26). The statistical details of these observations are given in the following sections.

The one-way ANOVA showed a significant main effect of concentrations on mouse CK-MM activity after incubation with PPD ($F_{5, 12} = 18.404$; $P < 0.01$), PPT ($F_{5, 12} = 6.301$; $P < 0.01$), and Rh2 ($F_{5,}$

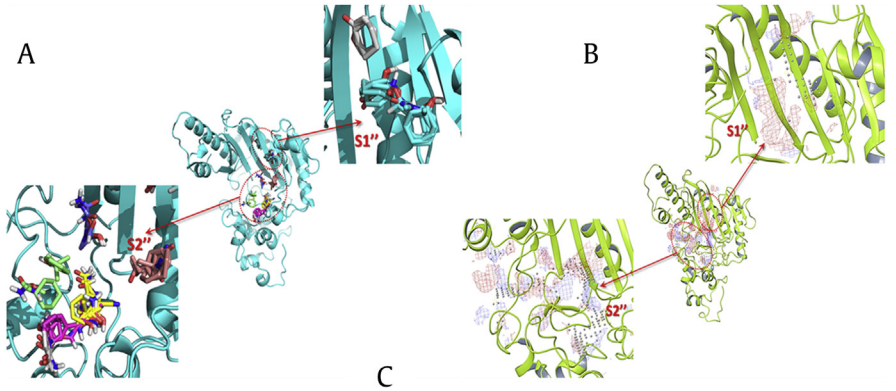

C

CK crystal	Docking Score	
	S1''	S2''
1I0E	-3.918	-5.005

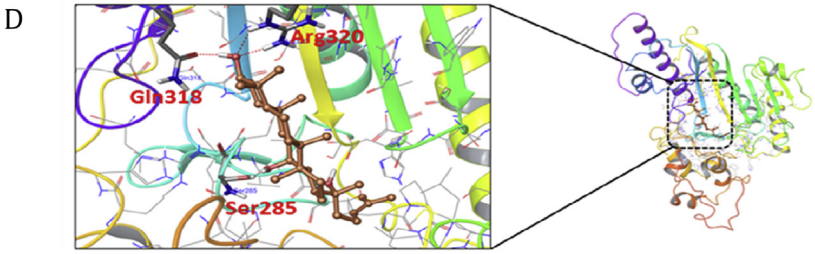

Fig. 4. Molecular docking studies on the human CK-MM/PPD complex. (A) Two potential binding sites (S1″ and S2″) on the surface of CK-MM were predicted by using the FTMap server. (B) SiteMap tool of Schrödinger software predicted the same binding sites as those obtained by FTMap analysis. (C) Docking conformation of PPD at each potential binding site was scored by the GlideScore tool. As the absolute value of docking score at the S2″ site was greater than that at the S1″ site, PPD was likely to bind to the S2″ site. (D) PPD docking to the S2″ site in the crystal structure of CK-MM. PPD was shown as a stick, with carbon atoms colored in brown, oxygen atoms colored in red, nitrogen atoms colored in blue, and hydrogen atoms colored in white. The key residues in CK-MM for binding were shown as sticks colored in gray. Intermolecular interactions were described using red dotted lines. CK-MM, muscle-type creatine kinase; PPD, 20(S)-protopanaxadiol.

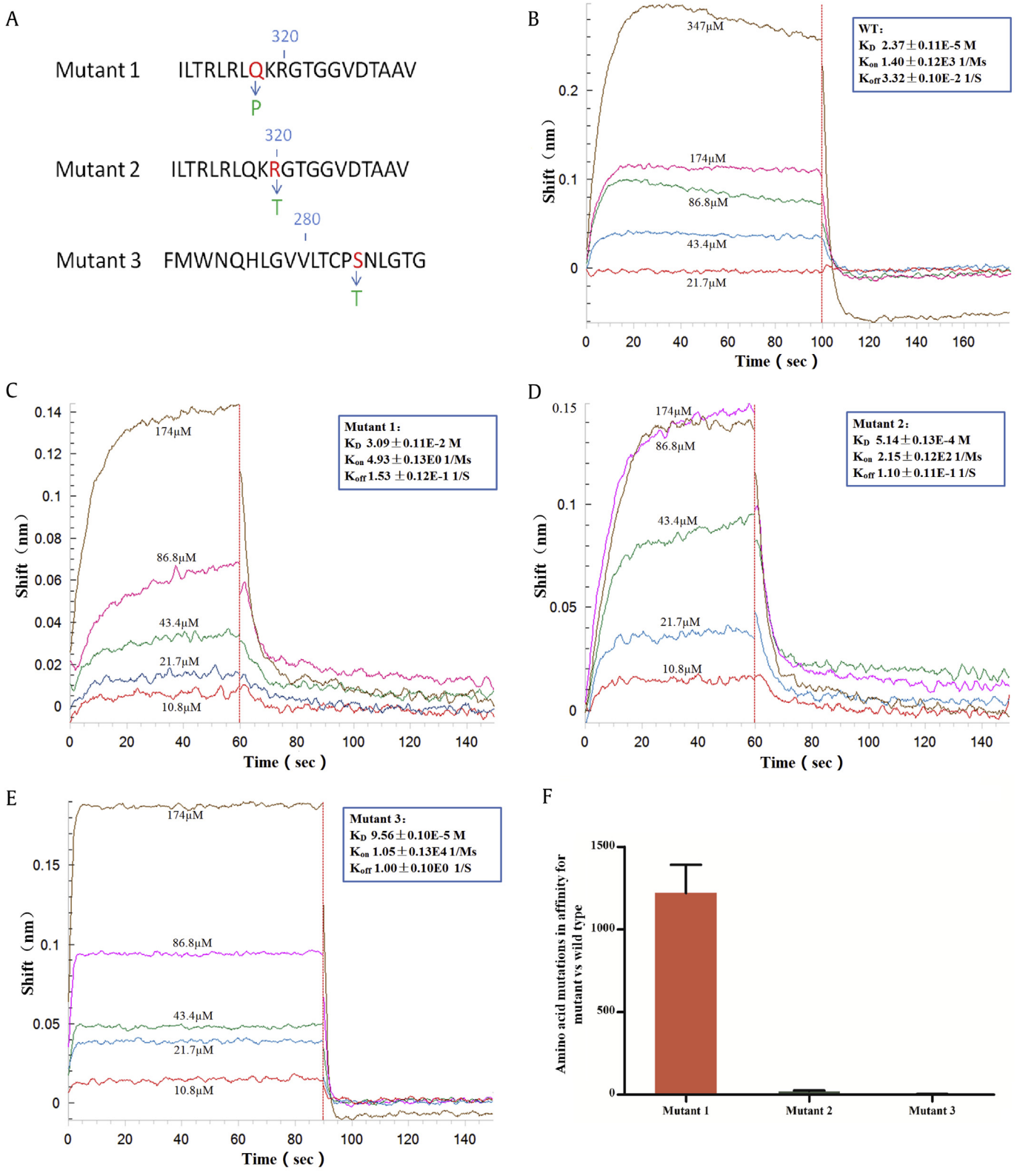

Fig. 5. Q318 residue was necessary for human CK-MM to achieve high affinity to PPD. (A) Three mutant forms of CK-MM, which have mutations of glutamine at Position 318 to proline (Q318P, Mutant 1), arginine at Position 320 to threonine (R320T, Mutant 2), and serine at Position 285 to threonine (S285T, Mutant 3), were generated using site-directed mutagenesis. (B) The binding of PPD to WT CK-MM (WT) was determined by the BLI technique. (C) The binding of Mutant 1 was determined by the BLI technique. (D) The binding of Mutant 2 was determined by the BLI technique. (E) The binding of Mutant 3 was determined by the BLI technique. Ni-Nitrilotriacetic acid (Ni-NTA) biosensors were loaded with His-tagged CK-MM and then incubated with PPD to generate an association curve. The 60-s association phase was subsequently followed by a 90-s dissociation step. The results presented are representative of at least three experiments. (F) Affinity (K_D) of Mutant 1 to PPD decreased dramatically, indicating that the Q318 residue was critical for the CK-MM/PPD complex. Data are expressed as mean ± SEM. ($n = 3$). BLI, biolayer interferometry; CK-MM, muscle-type creatine kinase; PPD, 20(S)-protopanaxadiol; PPT, protopanaxatriol; SEM, standard error of mean; WT, wild-type.

$_{12}$ = 6.241; $P < 0.01$). Multiple comparison tests further revealed that 10, 20, and 40 μM PPD incubations significantly increased mouse CK-MM activity by 4.2% ($P < 0.01$), 9.3% ($P < 0.01$), and 4.3% ($P < 0.01$), respectively. After incubation with PPT, mouse CK-MM activity significantly increased by 4.4%, 3.4%, and 2.1% at concentrations of 20 ($P < 0.05$), 40 ($P < 0.01$), and 80 μM ($P < 0.01$), respectively. A significant increase of mouse CK-MM activity was also observed after incubation with Rh2 at concentrations of 20 and 40 μM (3.1% [$P < 0.01$] and 3.5% [$P < 0.01$], respectively). However, no significant main effect of concentrations on mouse CK-MM activity was observed after incubation with Rg1 ($F_{5,\ 12}$ = 1.404; $P > 0.05$) and Rd ($F_{5,\ 12}$ = 1.241; $P > 0.05$) (Fig. 6A).

Regarding rabbit CK-MM activity, a significant main effect of concentrations was observed after incubation with PPD ($F_{5,\ 12}$ = 8.304; $P < 0.01$). Multiple comparison tests further revealed that 10, 20, and 40 μM PPD incubations significantly increased rabbit CK-MM activity by 7.0% ($P < 0.01$), 7.3% ($P < 0.05$), and 5.0% ($P < 0.05$), respectively (Fig. 6B). Meanwhile, PPD incubations increased human CK-MM activity, as shown by a significant main effect of concentrations ($F_{5,\ 12}$ = 6.407; $P < 0.01$). Multiple comparison tests further revealed that human CK-MM activity increased by 2.1%, 5.9%, and 2.4% at concentrations of 10 ($P < 0.05$), 20 ($P < 0.01$), and 40 μM ($P < 0.05$), respectively (Fig. 6C).

3.6. CK-MM activity in vivo

PPD was selected to further determine its effect on CK-MM activity *in vivo*. In general, daily p.o. PPD administration for 3 weeks slightly increased CK-MM activity in the skeletal muscle tissues of mice in a dose-dependent manner (Fig. 7A). Meanwhile, this treatment failed to produce an obvious impact on muscular CK-MM protein (Fig. 7B and C) and mRNA expression (Fig. 7D), which indicated that the direct interaction between PPD and CK-MM activated enzyme activity. The statistical details of these observations are given in the following sections.

One-way ANOVA test showed a significant main effect of groups on mouse CK-MM activity after p.o. PPD administration ($F_{3,\ 36}$ = 3.841; $P < 0.05$). Multiple comparison tests further revealed a tendency to increase CK-MM activity in skeletal muscle tissues of mice treated with PPD (50 mg/kg) daily for 3 weeks ($P = 0.079$). However, we found that 100 mg/kg PPD treatment significantly increased CK-MM activity by 4.83% compared with the control group ($P < 0.05$) (Fig. 7A). In addition, no significant main effect of groups on mouse CK-MM protein ($F_{3,\ 36}$ = 1.404; $P > 0.05$) and mRNA ($F_{3,\ 36}$ = 1.241; $P > 0.05$) expression was observed after p.o. PPD administration (Fig. 7B–D).

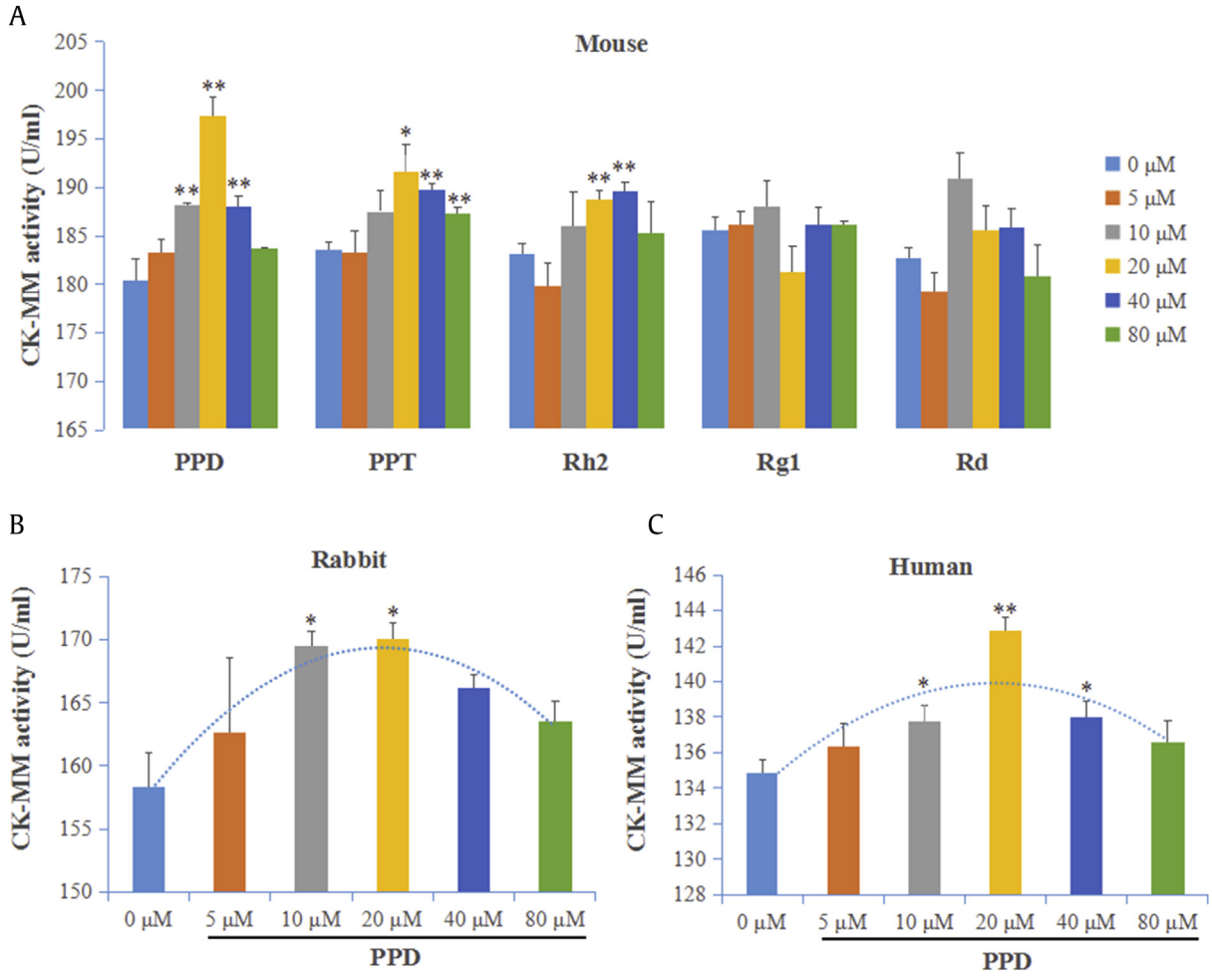

Fig. 6. Effects of ginsenosides and their aglycones on CK-MM activity *in vitro*. (A) Rg1 and Rd without direct interaction with CK-MM had no effects on mouse CK-MM activity. Rh2, PPT, and PPD significantly increased mouse CK-MM activity. Similarly, PPD significantly increased (B) rabbit and (C) human CK-MM activity and showed an inverted U-shaped effect. A detection kit was used to determine CK-MM activity, which in unknown samples was calculated using the standard curve and expressed as U/mL. Data are expressed as mean ± SEM. (n = 3) and analyzed by one-way ANOVA followed by Tukey's honest post hoc analysis. **P < 0.01, *P < 0.05 vs. the untreated CK-MM. ANOVA, analysis of variance; CK-MM, muscle-type creatine kinase; PPD, 20(S)-protopanaxadiol; PPT, protopanaxatriol; SEM, standard error of mean.

3.7. PPD dose-dependently increased the levels of tissue PCr and improved exercise performance in mice

CK catalyzes the reversible phosphoryl transfer reaction between ATP and creatine, producing ADP and PCr [33,34]. Given that PPD was able to activate CK-MM activity in skeletal muscles, we determined the effects of PPD on the muscular PCr content by using ion-pairing HPLC coupled to ultraviolet spectrometry analysis and mouse exercise performance in a weight-loaded swimming test.

One-way ANOVA test showed a significant main effect of groups on the muscular PCr content after p.o. PPD administration for 3 weeks ($F_{3, 36} = 5.601$; $P < 0.05$). Multiple comparison tests further revealed that daily treatment with 50 and 100 mg/kg PPD significantly increased PCr levels in skeletal muscles by 4.67% ($P < 0.05$) and 9.81% ($P < 0.01$) compared with the control group (Fig. 7E). In the weight-loaded swimming test, daily PPD administration for 3 weeks increased mouse endurance swimming time, as shown by a significant main effect of groups ($F_{3, 36} = 5.848$; $P < 0.01$). Multiple comparison tests further revealed a significant increase of endurance swimming time after p.o. administration with PPD doses of 50 and 100 mg/kg (37.3% [$P < 0.05$] and 42.5% [$P < 0.01$], respectively) (Fig. 7F).

3.8. PPD ameliorated the increase of lactate levels and decrease of ATP levels in skeletal muscles of mice induced by the 90-s weight-loaded swimming challenge

During intense exercise, serum or muscle lactate accumulation coincides with cellular acidosis and remains a good indicator of metabolic acidosis and muscle fatigue [35–37]. As described previously, PPD activated CK-MM activity and increased the muscular PCr content, indicating that PPD was able to strengthen the function of the CK/PCr system in the skeletal muscle. Then, we determined whether the function enhancement of the CK/PCr system improved cellular energy metabolism and retarded exercise-induced lactate accumulation to illustrate a mechanism by which PPD improved exercise performance in mice.

First, 90 s of the swimming challenge induced a significant increase in muscle lactate levels compared with the control group ($P < 0.01$). Three weeks of daily PPD preventive administration significantly reversed the increase in muscle lactate levels ($P < 0.05$) (Fig. 8A). Two-way ANOVA showed the significant effects of swim ($F_{1, 36} = 7.540$; $P < 0.05$) and drug treatment ($F_{1, 36} = 3.947$; $P < 0.05$) with a significant interaction between these factors ($F_{1, 36} = 15.638$; $P < 0.01$). Muscle ADP levels were also significantly increased in the mice of the swim and PPD + swim groups. Two-way ANOVA revealed a highly significant main effect of swim ($F_{1, 36} = 9.678$; $P < 0.01$) but not of drug treatment ($F_{1, 36} = 1.241$; $P > 0.05$) (Fig. 8B).

Second, two-way ANOVA revealed significant changes in muscle ATP levels, with a significant main effect of swim ($F_{1, 36} = 6.745$; $P < 0.05$) and drug treatment ($F_{1, 36} = 3.447$; $P < 0.05$) with a significant interaction between these factors ($F_{1, 36} = 3.6478$; $P < 0.05$). Multiple comparison tests further revealed that daily PPD preventive administration significantly reversed the decrease of muscle ATP levels induced by 90 s of the swimming challenge ($P < 0.01$) (Fig. 8C). Similar to muscle ATP levels, PPD administration significantly blocked the decrease of muscle ATP/ADP induced

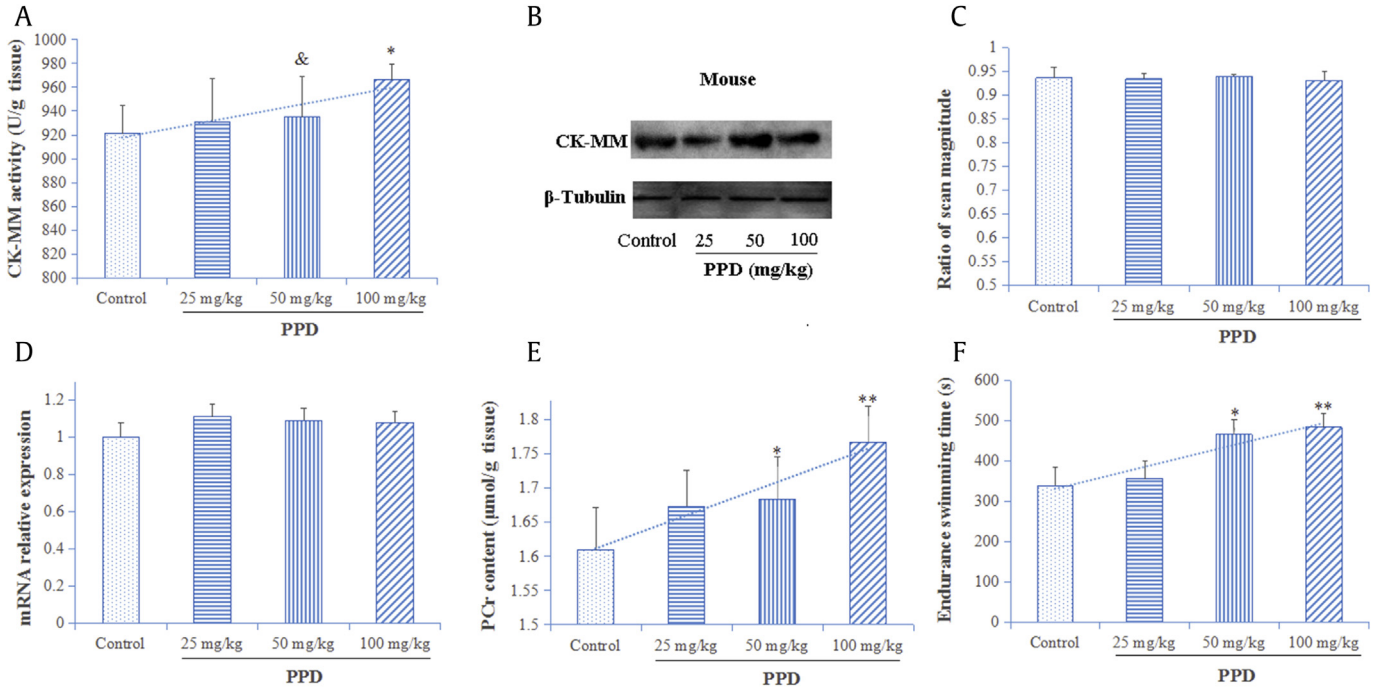

Fig. 7. PPD enhanced the CK/PCr system functions by activating CK-MM activity in the skeletal muscle tissues of mice. (A) PPD was administered daily profess to be convinced (p.o.) to the mice, and the control group of mice was given the vehicle. After treatment for 3 weeks, CK-MM activity in skeletal muscle tissues was calculated using the standard curve of purified mouse CK-MM following the manufacturer's protocol and expressed as U/g skeletal muscle tissue (mean ± SEM, $n = 10$). (B) CK-MM protein levels were determined by Western blot analysis. (C) Values of CK-MM levels were normalized against the amount of β-tubulin (mean ± SEM, $n = 10$). (D) Muscular CK-MM mRNA levels were determined by real-time PCR, and relative expression was calculated using the $2^{-\Delta\Delta Ct}$ method (mean ± SEM, $n = 10$). (E) PCr content in skeletal muscle tissues was measured using ion-pairing HPLC–UV and expressed as nmol/g skeletal muscle tissue (mean ± SEM, $n = 10$). (F) PPD dose-dependently improved exercise performance in mice. After daily p.o. administration for 3 weeks, the mice were subjected to the weight-loaded swimming test. The swimming endurance time was recorded from the beginning to exhaustion (mean ± SEM, n = 10). Data were analyzed by one-way ANOVA followed by Tukey's honest post hoc analysis. $^{**}P < 0.01$, $^{*}P < 0.05$ vs. control; $^{\&}P = 0.079$ vs. control. ANOVA, analysis of variance; CK-MM, muscle-type creatine kinase; HPLC, high-performance liquid chromatography; PCR, polymerase chain reaction; PCr, phosphocreatine; PPD, 20(S)-protopanaxadiol; PPT, protopanaxatriol; SEM, standard error of mean.

by the acute swimming challenge ($P < 0.05$) (Fig. 8D). Two-way ANOVA showed the significant effects of swim ($F_{1, 36} = 9.243$; $P < 0.01$) and drug treatment ($F_{1, 36} = 3.342$; $P < 0.05$) with a significant interaction between these factors ($F_{1, 36} = 3.638$; $P < 0.05$).

Third, significant effects of swim ($F_{1, 36} = 11.570$; $P < 0.01$) and drug treatment ($F_{1, 36} = 9.914$; $P < 0.01$) were observed on the muscle PCr content with a significant interaction between these factors ($F_{1, 36} = 8.614$; $P < 0.01$). Multiple comparison tests further revealed that daily PPD preventive administration alone significantly increased the PCr content in muscle tissue compared with the control group ($P < 0.05$) but had no effects on the decrease of the muscle PCr content induced by the acute swimming challenge (Fig. 8E). As for PCr/ATP, daily PPD preventive administration significantly promoted the decrease of the muscle PCr/ATP content induced by the acute swimming challenge ($P < 0.05$). However, PPD treatment alone significantly increased the muscle PCr/ATP content compared with the control group ($P < 0.05$) (Fig. 8F). Two-way ANOVA showed the significant effects of swim ($F_{1, 36} = 31.135$; $P < 0.01$) and drug treatment ($F_{1, 36} = 3.675$; $P < 0.05$) with a significant interaction between these factors ($F_{1, 36} = 14.273$; $P < 0.01$).

4. Discussion

The identification of the protein targets of natural products is very important for understanding the action mechanisms to develop natural products for use as therapeutic drugs [38,39]. Although various new strategies without chemical modification have recently been developed to identify the target proteins of natural products (i.e., drug affinity responsive target stability [40], cellular thermal shift [41], and stability of proteins from rates of oxidation [42]), affinity chromatography remains the most widely used method [19,43,44]. Compared with newly developed target identification methods [45,46], the advantage of affinity-based methods is that they rely solely on binding of the compound to its target proteins rather than on specific biochemical readouts (i.e., thermodynamic [47]or proteolytic [48] measurements) that may be only useful for a fraction of compounds. However, as for affinity chromatography, the functional groups of natural products have to be used as points of attachment to the solid matrix through chemical modification. If these functional groups or their removal after metabolism is essential for compound bioactivity, the shadowing of these sites by using labeling procedures produces obstacles in identifying target proteins [19,45].

Consequently, we used high-purity ginseng total saponins as the ligand, in which the ginsenosides differ from one another by the site of sugar attachment at Positions C-3, C-6, or C-20 (Supplementary Fig. 1), to ensure the chance of each site being revealed and bound while incubating with protein extracts. Nearly 40 proteins were finally identified as potential targets of ginsenosides, from which validating the direct targets is often the most challenging and time-consuming step. Besides luck, it was easier to validate CK-MM as the direct target of ginsenosides in skeletal muscle tissues probably because of the following strategies. Affinity beads were used to pull down the binding proteins not only from

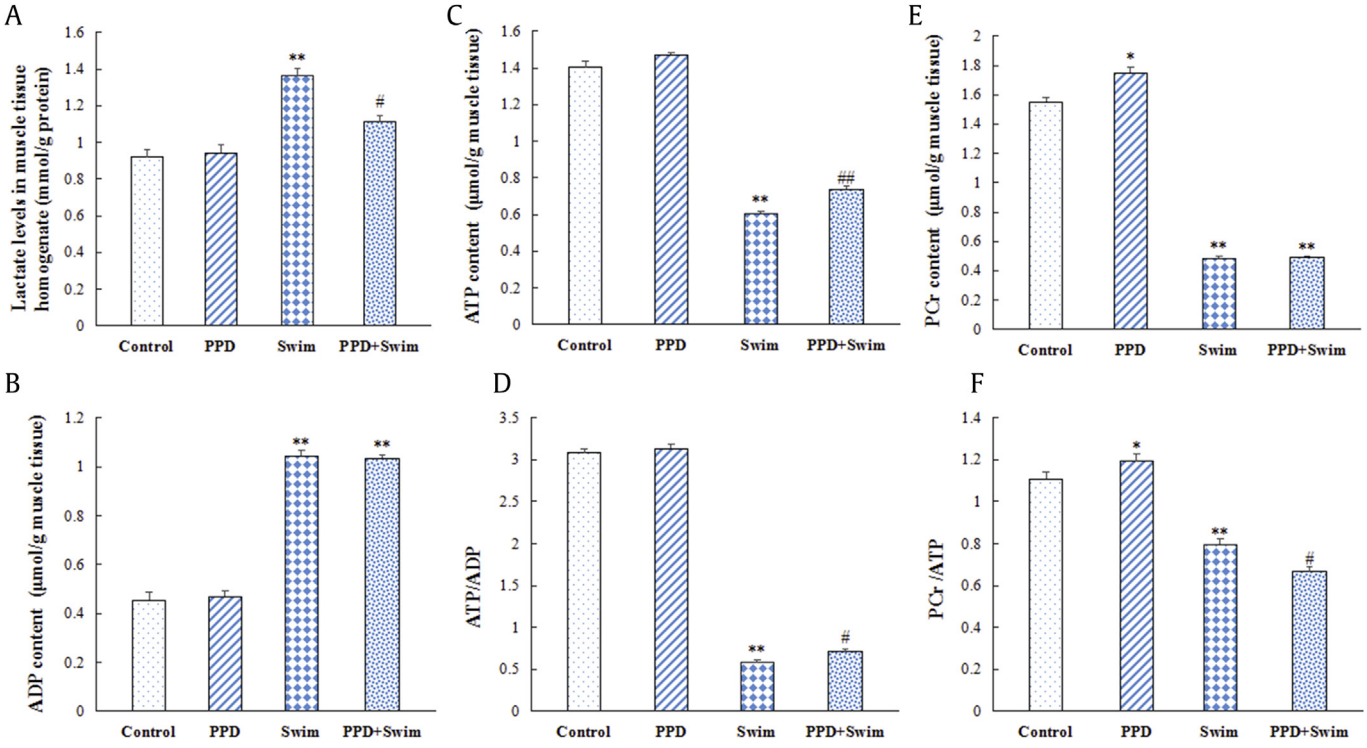

Fig. 8. PPD improved cellular energy metabolism and retarded exercise-induced lactate accumulation. (A) After daily profess to be convinced (p.o.) administration (100 mg/kg/day) for 3 weeks, the mice were subjected to the weight-loaded swimming for 90 s. The lactate levels in muscle tissue homogenate were measured using the commercial kits. The unknown sample level was determined from the standard curve and expressed as mmol lactate per mg protein (mean ± SEM, $n = 10$). The (B) ADP and (C) ATP contents in skeletal muscle tissues were measured using ion-pairing HPLC–UV and expressed as nmol/g skeletal muscle tissue (mean ± SEM, $n = 10$). (D) Ratio of ATP to ADP was calculated (mean ± SEM, $n = 10$). (E) PCr content in skeletal muscle tissues was also measured using ion-pairing HPLC–UV and expressed as nmol/g skeletal muscle tissue (mean ± SEM, $n = 10$). (F) Ratio of PCr to ATP was calculated (mean ± SEM, $n = 10$). Data were analyzed by two-way ANOVA with treatment and swim as factors. $^{**}P < 0.01$, $^{*}P < 0.05$ vs. control; $^{\#\#}P < 0.01$, $^{\#}P < 0.05$ vs. swim, Tukey's honest significant difference test. ANOVA, analysis of variance; HPLC, high-performance liquid chromatography; PCr, phosphocreatine; PPD, 20(S)-protopanaxadiol; SEM, standard error of mean.

muscle tissue extracts but also from other target tissue extracts (i.e., brain, spleen, stomach, and intestine). Brain-type CK was also included in potential target proteins of ginsenosides with top Mascot score in brain tissues (Supplementary Fig. 23), which attracted our attention to CK-MM. In addition, we used the BLI technique to determine the direct binding response of CK-MM to not only parent ginsenosides (i.e., Rg1, Re, Rb1, and Rd) but also their metabolites (i.e., Rh1, Rh2, F1, GK, PPT, and PPD). If we only assessed the direct interaction between CK-MM and parent ginsenosides, the CK-MM target might be missed.

In subsequent studies, we selected PPD as a representative to confirm direct binding and its biological importance, which displayed the strongest interaction with CK-MM in parent ginsenosides and their metabolites. We demonstrated the direct interaction between PPD and recombinant human CK-MM by BLI kinetics analysis (Fig. 3C). The ITC assays further confirmed that PPD specifically bound to human CK-MM (Fig. 3D). Molecular docking suggested that PPD can be docked successively into the active site (S2″) adjacent to the ADP binding pocket (S1″) on the crystal structure of human CK-MM (Fig. 4D). In addition, the mutation of key amino acids (R320 and S285) in the S2″ site decreased the affinity between PPD and CK-MM by BLI kinetics analysis, and the mutation at Q318 almost caused the loss of PPD binding (Fig. 5). These results demonstrated that CK-MM was a cellular target of PPD and that the S2″ pocket was a site in the engagement between CK-MM and ginsenosides.

We then observed the effects of PPD on CK-MM activity. PPD was found to significantly increase human, mouse, and rabbit CK-MM activity *in vitro* (Fig. 6). In addition, PPT and Rh2 also significantly increased the mouse CK-MM activity, whereas Rg1 and Rd (two representatives of parent ginsenosides), without the binding to CK-MM, produced no effects on mouse CK-MM activity (Fig. 6A). Furthermore, correlation analysis showed that the maximum increase of the rate of enzyme activity was well correlated with the direct binding response of representative ginsenosides and aglycones to CK-MM (Supplementary Fig. 26). These results indicated that the S2″ pocket might be an activation center of CK-MM, to which Rh2, PPT, and PPD bound, called allosteric activators. Interestingly, Rh2, PPT, and PPD showed an inverted U-shaped effect on CK-MM activity *in vitro* (Fig. 6B and C). The inverted U-shaped dose response was frequently found in the studies of small molecular compounds' bioactivity (i.e., 17-beta-estradiol [49], dopamine [50], nicotine [51], and cannabidiol [52]), which was generally explained by their different receptors. For example, low levels of 17-beta-estradiol will mostly activate the high-affinity estrogen receptor α (activating synaptogenesis), whereas high 17-beta-estradiol levels activate low-affinity estrogen receptor β (decreasing synaptogenesis) [49]. In the study, CK-MM was found to have two potential active sites (S1″ and S2″) using FTMap (Fig. 4A) and SiteMap (Fig. 4B) software. Although Glide software analysis failed to successively dock PPD into the S1″ site, we speculated that high levels of PPD might disturb the ADP binding site (S1″) and produce adverse impact on CK-MM activity, which still need to be elucidated in future studies. However, 3-week PPD administration (25, 50, and 100 mg/kg/day) dose-dependently activated CK-MM activity in the skeletal muscle tissues of mice (Fig. 7A). Based on our findings *in vitro*, more than 20 μM PPD incubation might produce adverse impact on CK-MM activity. Meanwhile, the plasma peak concentration in rats was less than 10 μM after oral administration once with PPD suspension (100 mg/kg) in the pharmacokinetic studies by Wang et al. [53], which was located in the upward section of the inverted U-shaped concentration–effect curves.

Moreover, the increase of CK-MM activity caused by PPD administration was accompanied by an increase in PCr tissue levels. Several previous studies have indicated the relationship between CK-MM activity and PCr level in tissues. For example, PCr levels were decreased in skeletal muscles of mice deficient in both cytosolic and mitochondrial CK activities [54,55]. In the study by Dzeja et al. [56], tracking perturbations in metabolic dynamics demonstrated that hearts lacking muscle-type CK had low PCr turnover. Inversely, muscle-type CK overexpression significantly improved PCr recovery in mouse hearts after ischemia and reperfusion [57]. In the present study, after 3-week PPD treatment (100 mg/kg), CK-MM activity and PCr levels in the skeletal muscle were increased by 4.83% and 9.81%, respectively (Fig. 7A and E). Although the increment of CK-MM activity and PCr levels was not very high, it could significantly delay lactate accumulation induced by the 90-s exercise challenge (Fig. 8A) and substantially improve mouse exercise performance in a weight-loaded swimming test (Fig. 7F). Several possible biological mechanisms for the efficacy are discussed in the following paragraphs.

First, in the skeletal muscle of PPD-treated mice, the ATP content remained the same as in the control mice (Fig. 8C), but the PCr content and PCr/ATP ratio increased compared with the control group (Fig. 8E and F). As an efficient highway connecting ATP production and consumption sites, the CK/PCr system facilitates the transfer of high-energy phosphates from the mitochondria (where ATP is produced) to myofibrils (where ATP is consumed) and enables the return of products to the mitochondria for rephosphorylation [33,34,58]. Thus, high PCr concentrations, PCr/ATP ratio, and CK-MM activity mean not only increased energy stores in the body but also enhanced regeneration of ATP by the CK/PCr system in microdomains, which are critically important for the function of the skeletal muscle [59]. In case of high rates of energy demand or oxygen deficiency, the enhanced CK/PCr system was thus more beneficial to buffer cellular ATP as reflected by the increased ATP/ADP ratio (Fig. 8D) and decreased PCr/ATP ratio (Fig. 8F) compared with the swim group. Notably, the occurrence of glycolysis, which causes metabolic acidosis and lactate accumulation, is due to decreased steady-state levels of ATP (i.e., a rate of ATP demand exceeds ATP supply from oxidative phosphorylation) [60,61]. Defending ATP concentration by virtue of PCr might delay the occurrence of glycolysis and then reduce fatigue and improve exercise performance. Second, the CK reaction is alkalinizing to the cell as a proton is consumed in this reaction [33,62,63]. The proton is required to replace the phosphate group of creatine phosphate, completing the second amine functional group of creatine [35]. As a buffer of protons, enhancement of the CK/PCr system indicated that the protons released from the reaction of glycolysis can be eliminated by the CK reaction, which was helpful to relieve metabolic acidosis. Finally, vigorous or resistance exercise can result in localized damage to muscle tissue, and a resulting increase in membrane permeability is observed [64,65]. The increased membrane permeability allows CK-MM to leak into interstitial fluid, where it then enters circulation [66]. The increment of CK-MM activity induced by PPD was likely to counteract the decrease of intracellular CK-MM levels because of its leakage and then to keep intracellular CK-MM activity to help fatigue recovery [57].

5. Conclusion

We demonstrated here that CK-MM is a target of ginsenosides in the muscle. Parent ginsenoside metabolites directly bind to CK-MM and activate its activity. This activation increases the levels of tissue PCr, enhances regeneration of ATP by the CK/PCr system in microdomains, and thus retards exercise-induced lactate accumulation. To our knowledge, this study is the first to discover small-molecule activators of CK-MM. Our findings contribute to a better understanding of the action mechanisms of ginseng antifatigue effect and produce relevant implications in developing better

CK-MM activators based on the dammarane-type triterpenoid structure with a four *trans*-ring rigid steroid skeleton.

6. Contributors

Feiyan Chen designed and purified CK-MM mutants and conducted the *in vitro* binding assays; Kexuan Zhu designed and conducted the *in vivo* animal experiments and undertook biochemical measurement; Lin Chen prepared the figures and supplementary material and wrote the draft of the manuscript; Liufeng Ouyang prepared high-purity ginseng total saponins and conducted affinity chromatography experiments; Cuihua Chen carried out HPLC analysis; Ling Gu and Yucui Jiang assisted in biochemical measurement; Zhongli Wang assisted in target identification; Jianguo Dai selected the statistical methods and performed the data analysis; Zixuan Lin, Qiang Zhang, and Xiao Shao assisted in the data analysis; Yunan Zhao conceived the idea for this project, supervised, and supported the project; and all authors discussed the results and commented on the manuscript.

Conflicts of interest

The authors have declared that there is no conflict of interest.

Acknowledgments

The study was financially supported by National Natural Science Foundation of China (Nos. 81873025, 81703732) and Jiangsu Provincial Natural Science Foundation of China (BK20181423). The authors thank Dr Daqing Gao from the Southeast University of China for her gifts of *E. coli* BL-21 cells and vector pET-28a.

Appendix A. Supplementary data

Supplementary data to this article can be found online at https://doi.org/10.1016/j.jgr.2019.02.005.

References

[1] Helms S. Cancer prevention and therapeutics: Panax ginseng. Altern Med Rev 2004;9:259–74.
[2] Choi KT. Botanical characteristics, pharmacological effects and medicinal components of Korean Panax ginseng C A Meyer. Acta Pharmacol Sin 2008;29:1109–18.
[3] Yun TK. Panax ginseng–a non-organ-specific cancer preventive? Lancet Oncol 2001;2:49–55.
[4] Baeg IH, So SH. The world ginseng market and the ginseng (Korea). J Ginseng Res 2013;37:1–7.
[5] Shin BK, Kwon SW, Park JH. Chemical diversity of ginseng saponins from Panax ginseng. J Ginseng Res 2015;39:287–9.
[6] Qi LW, Wang CZ, Du GJ, Zhang ZY, Calway T, Yuan CS. Metabolism of ginseng and its interactions with drugs. Curr Drug Metab 2011;12:818–22.
[7] Peng D, Wang H, Qu C, Xie L, Wicks SM, Xie J. Ginsenoside Re: its chemistry, metabolism and pharmacokinetics. Chin Med 2012;7:2.
[8] Ma GD, Chiu CH, Hsu YJ, Hou CW, Chen YM, Huang CC. Changbai mountain ginseng (Panax ginseng C.A. Mey) extract supplementation improves exercise performance and energy utilization and decreases fatigue-associated parameters in mice. Molecules 2017;22:237.
[9] Oh HA, Kim DE, Choi HJ, Kim NJ, Kim DH. Anti-fatigue effects of 20(S)-protopanaxadiol and 20(S)-protopanaxatriol in mice. Biol Pharm Bull 2015;38:1415–9.
[10] Choi JY, Woo TS, Yoon SY, Ike Campomayor Dela P, Choi YJ, Ahn HS, Lee YS, Yu GY, Cheong JH. Red ginseng supplementation more effectively alleviates psychological than physical fatigue. J Ginseng Res 2011;35:331–8.
[11] Tan SJ, Li N, Zhou F, Dong QT, Zhang XD, Chen BC, Yu Z. Ginsenoside Rb1 improves energy metabolism in the skeletal muscle of an animal model of postoperative fatigue syndrome. J Surg Res 2014;191:344–9.
[12] Lee N, Lee SH, Yoo HR, Yoo HS. Anti-fatigue effects of enzyme-modified ginseng extract: a randomized, double-blind, placebo controlled trial. J. Altern Complement Med 2016;22:859–64.
[13] Kim HG, Cho JH, Yoo SR, Lee JS, Han JM, Lee NH, Ahn YC, Son CG. Antifatigue effects of Panax ginseng C.A. Meyer: a randomised, double-blind, placebo-controlled trial. PLoS One 2013;8:e61271.
[14] Lee NH, Jung HC, Lee S. Red ginseng as an ergogenic aid: a systematic review of clinical trials. J Exerc Nutrition Biochem 2016;20:13–9.
[15] Arring NM, Millstine D, Marks LA, Nail LM. Ginseng as a treatment for fatigue: a systematic review. J Altern Complement Med 2018;24:624–33.
[16] Bach HV, Kim J, Myung SK, Cho YA. Efficacy of ginseng supplements on fatigue and physical performance: a Meta-analysis. J Korean Med Sci 2016;31:1879–86.
[17] Bae JW, Lee MH. Effect and putative mechanism of action of ginseng on the formation of glycated hemoglobin in vitro. J Ethnopharmacol 2004;91:137–40.
[18] Li Z, Chen X, Niwa Y, Sakamoto S, Nakaya Y. Involvement of Ca^{2+} activated K^{+} channels in ginsenosides-induced aortic relaxation in rats. J Cardiovasc Pharmacol 2001;37:41–7.
[19] Lomenick B, Olsen RW, Huang J. Identification of direct protein targets of small molecules. ACS Chem Biol 2011;6:34–46.
[20] Zhao YN, Wang ZL, Dai JG, Chen L, Huang YF. Preparation and quality assessment of high-purity ginseng total saponins by ion exchange resin combined with macroporous adsorption resin separation. Chin J Nat Med 2014;12:382–92.
[21] Ouyang LF, Wang ZL, Dai JG, Chen L, Zhao YN. Determination of total ginsenosides in ginseng extracts using charged aerosol detection with post-column compensation of the gradient. Chin J Nat Med 2014;12:857–68.
[22] Joo EJ, Ha YW, Shin H, Son SH, Kim YS. Generation and characterization of monoclonal antibody to ginsenoside Rg3. Biol Pharma Bull 2009;32:548–52.
[23] Leung SM, Pitts RL. A novel approach using MALDI-TOF/TOF mass spectrometry and prestructured sample supports (AnchorChip Technology) for proteomic profiling and protein identification. Methods Mol Biol 2008;441:57–70.
[24] Brosch M, Yu L, Hubbard T, Choudhary J. Accurate and sensitive peptide identification with Mascot percolator. J Proteome Res 2009;8:3176–81.
[25] Li J, Schantz A, Schwegler M, Shankar G. Detection of low-affinity anti-drug antibodies and improved drug tolerance in immunogenicity testing by Octet® biolayer interferometry. J Pharm Biomed Anal 2011;54:286–94.
[26] Ladbury JE, Chowdhry BZ. Sensing the heat: the application of isothermal titration calorimetry to thermodynamic studies of biomolecular interactions. Chem Biol 1996;3:791–801.
[27] Zhao YN, Zhang Q, Shao X, Ouyang LF, Wang X, Zhu KX, Chen L. Decreased glycogen content might contribute to chronic stress induced atrophy of hippocampal astrocyte volume and depression like behavior in rats. Sci Rep 2017;7:43192.
[28] Xu L, Wang CY, Lv L, Liu KX, Sun HJ, Han GZ. Pharmacokinetics of phosphocreatine and its active metabolite creatine in the mouse plasma and myocardium. Pharmacol Rep 2014;66:908–14.
[29] Di Pierro D, Tavazzi B, Perno CF, Bartolini M, Balestra E, Caliò R, Giardina B, Lazzarino G. An ion-pairing high-performance liquid chromatographic method for the direct simultaneous determination of nucleotides, deoxynucleotides, nicotinic coenzymes, oxypurines, nucleosides, and bases in perchloric acid cell extracts. Anal Biochem 1995;231:407–12.
[30] Concepcion J, Witte K, Wartchow C, Choo S, Yao D, Persson H, Wei J, Li P, Heidecker B, Ma W, et al. Label-free detection of biomolecular interactions using biolayer interferometry for kinetic characterization. Comb Chem High Throughput Screen 2009;12:791–800.
[31] Callies O, Hernández Daranas A. Application of isothermal titration calorimetry as a tool to study natural product interactions. Nat Prod Rep 2016;33:881–904.
[32] Lahiri SD, Wang PF, Babbitt PC, McLeish MJ, Kenyon GL, Allen KN. The 2.1 Å structure of *Torpedo californica* creatine kinase complexed with the ADP-Mg^{2+}-NO^{3-}-creatine transition-state analogue complex. Biochemistry 2002;41:13861–7.
[33] Wallimann T, Tokarska-Schlattner M, Schlattner U. The creatine kinase system and pleiotropic effects of creatine. Amino Acids 2011;40:1271–96.
[34] Sahlin K, Harris RC. The creatine kinase reaction: a simple reaction with functional complexity. Amino Acids 2011;40:1363–7.
[35] Robergs RA, Ghiasvand F, Parker D. Biochemistry of exercise-induced metabolic acidosis. Am J Physiol Regul Intergr Comp Physiol 2004;287:R502–16.
[36] Hall MM, Rajasekaran S, Thomsen TW, Peterson AR. Lactate: friend or foe. PM R 2016;8:S8–15.
[37] Adeva-Andany M, López-Ojén M, Funcasta-Calderón R, Ameneiros-Rodríguez E, Donapetry-García C, Vila-Altesor M, Rodríguez-Seijas J. Comprehensive review on lactate metabolism in human health. Mitochondrion 2014;17:76–100.
[38] McFedries A, Schwaid A, Saghatelian A. Methods for the elucidation of protein-small molecule interactions. Chem Biol 2013;20:667–73.
[39] Rask-Andersen M, Masuram S, Schioth HB. The druggable genome: evaluation of drug targets in clinial trials suggests major shifts in molecular class and indication. Annu Rev Pharmacol Toxicol 2014;54:9–26.
[40] Lomenick B, Hao R, Jonai N, Chin RM, Aghajan M, Warburton S, Wang J, Wu RP, Gomez F, Loo JA, et al. Target identification using drug affinity responsive target stability (DARTS). PNAS 2009;106:21984–9.
[41] Martinez Molina D, Jafari R, Ignatushchenko M, Seki T, Larsson EA, Dan C, Sreekumar L, Cao Y, Nordlund P. Monitoring drug target engagement in cells and tissues using the cellular thermal shift assay. Science 2013;341:84–7.
[42] Strickland EC, Geer MA, Tran DT, Adhikari J, West GM, DeArmond PD, Xu Y, Fitzgerald MC. Thermodynamic analysis of protein-ligand binding interactions

in complex biological mixtures using the stability of proteins from rates of oxidation. Nat Protoc 2013;8:148–61.
[43] Ong SE, Li X, Schenone M, Schreiber SL, Carr SA. Identifying cellular targets of small-molecule probes and drugs with biochemical enrichment and SILAC. Methods Mol Biol 2012;803:129–40.
[44] Ziegler S, Pries V, Hedberg C, Waldmann H. Target identification for small bioactive molecules: finding the needle in the haystack. Angew Chem Int Ed Engl 2013;52:2744–92.
[45] Chang J, Kim Y, Kwon HJ. Advances in identification and validation of protein targets of natural products without chemical modification. Nat Prod Rep 2016;33:719–30.
[46] Futamura Y, Muroi M, Osada H. Target identification of small molecules based on chemical biology approaches. Mol Biosyst 2013;9:897–914.
[47] Huber KV, Olek KM, Müller AC, Tan CS, Bennett KL, Colinge J, Superti-Furga G. Proteome-wide drug and metabolite interaction mapping by thermal-stability profiling. Nat Methods 2015;12:1055–7.
[48] Pai MY, Lomenick B, Hwang H, Schiestl R, McBride W, Loo JA, Huang J. Drug affinity responsive target stability (DARTS) for small molecule target identification. Methods Mol Biol 2015;1263:287–98.
[49] Bayer J, Gläscher J, Finsterbusch J, Schulte LH, Sommer T. Linear and inverted U-shaped dose-response functions describe estrogen effects on hippocampal activity in young women. Nat Commun 2018;9:1220.
[50] Cools R, D'Esposito M. Inverted-U-shaped dopamine actions on human working memory and cognitive control. Biol Psychiatry 2011;69:e113–25.
[51] Ashor AW. Inverted U shaped effect of nicotine on the severity of depressive symptoms: a population-based survey. J Young Pharm 2013;5:60–3.
[52] Zuardi AW, Rodrigues NP, Silva AL, Bernardo SA, Hallak JEC, Guimarães FS, Crippa JAS. Inverted U-shaped dose-response curve of the anxiolytic effect of cannabidiol during public speaking in real life. Front Pharmacol 2017;8:259.
[53] Wang B, Pu Y, Xu B, Tao J, Wang Y, Zhang T, Wu P. Self-microemulsifying drug delivery system improved oral bioavailability of 20(S)-protopanaxadiol: from preparation to evaluation. Chem Pharm Bull (Tokyo) 2015;63:688–93.
[54] Steeghs K, Benders A, Oerlemans F, de Haan A, Heerschap A, Ruitenbeek W, Jost C, van Deursen J, Perryman B, Pette D. Altered Ca^{2+} responses in muscles with combined mitochondrial and cytosolic creatine kinase deficiencies. Cell 1997;89:93–103.
[55] In't Zandt HJ, de Groof AJ, Renema WK, Oerlemans FT, Klomp DW, Wieringa B, Heerschap A. Presence of (phospho)creatine in developing and adult skeletal muscle of mice without mitochondrial and cytosolic muscle creatine kinase isoforms. J Physiol 2003;548:847–58.
[56] Dzeja PP, Hoyer K, Tian R, Zhang S, Nemutlu E, Spindler M, Ingwall JS. Rearrangement of energetic and substrate utilization networks compensate for chronic myocardial creatine kinase deficiency. J Physiol 2011;589:5193–211.
[57] Akki A, Su J, Yano T, Gupta A, Wang Y, Leppo MK, Chacko VP, Steenbergen C, Weiss RG. Creatine kinase overexpression improves ATP kinetics and contractile function in postischemic myocardium. Am J Physiol Heart Circ Physiol 2012;303:H844–52.
[58] Kitzenberg D, Colgan SP, Glover LE. Creatine kinase in ischemic and inflammatory disorders. Clin Trans Med 2016;5:31.
[59] Guzun G, Timohhina N, Tepp K, Gonzalez-Granillo M, Shevchuk I, Chekulayev V, Kuznetsov AV, Kaambre T, Saks VA. Systems bioenergetics of creatine kinase networks: physiological roles of creatine and phosphocreatine in regulation of cardiac cell function. Amino Acids 2011;40:1333–48.
[60] Lindinger MI, Kowalchuk JM, Heigenhauser GJ. Applying physicochemical principles to skeletal muscle acid-base status. Am J Physiol Regul Intergr Comp Physiol 2005;289:R891–4.
[61] Van Hall G. Lactate kinetics in human tissues at rest and during exercise. Acta Physiol (Oxf) 2010;199:499–508.
[62] Wallimann T, Wyss M, Brdiczka D, Nicolay K, Eppenberger HM. Intracellular compartmentation, structure and function of creatine kinase isoenzymes in tissues with high and fluctuating energy demands: the 'phosphocreatine circuit' for cellular energy homeostasis. Biochem J 1992;281(1):21–40.
[63] Wallimann T, Tokarska-Schlattner M, Neumann D, Epand RM, Epand RF, Andres RH, Widmer H. The phospho-creatine circuit: molecular and cellular physiology of creatine kinases, sensitivity to free radicals and enhancement by creatine supplementation. In: Saks VA, editor. Molecular systems bioenergetics: energy for life. Weinheim: Wiley; 2007. p. 195–264.
[64] Clarkson PM, Sayers SP. Etiology of exercise-induced muscle damage. Can J Appl Physiol 1999;24:234–48.
[65] Koch AJ, Pereira R, Machado M. The creatine kinase response to resistance exercise. J Musculoskelet Neuronal Interact 2014;14:68–77.
[66] Brancaccio P, Lippi G, Maffulli N. Biochemical markers of muscular damage. Clin Chem Lab Med 2010;48:757–67.